Nobel Metal Based High Entropy Alloy for Conversion of Carbon-di-oxide (CO_2) to Hydrocarbon

Subramanian Nellaiappan[†‡], Nirmal Kumar[§‡], Ritesh Kumar[ζ‡], Arko Parui[ζ], Kirtiman Deo Malviya[ϒ], K. G. Pradeep[׀], Abhishek K. Singh[ζ]*, Sudhanshu Sharma[†]*, Chandra Sekhar Tiwary[Ψ]*, Krishanu Biswas[§]*

[†]*Department of Chemistry, Indian Institute of Technology Gandhinagar, Gandhinagar - 382355, INDIA; Email: ssharma@iitgn.ac.in*

[§]*Department of Materials Science and Engineering, Indian Institute of Technology Kanpur, Kanpur-208016, INDIA; Email: kbiswas@iitk.ac.in*

[ζ]*Materials Research Center, Indian Institute of Science, Bangalore-560012, INDIA; Email: abhishek@iisc.ac.in*

[ϒ]*Department of Materials Engineering, Indian Institute of Science, Bangalore-560012, INDIA*

[׀]*Department of Materials Science and Metallurgical Engineering, Indian Institute of Technology Madras, Chennai-600036, INDIA*

[Ψ]*Metallurgical and Materials Engineering, Indian Institute of Technology Kharagpur, Kharagpur-382355, INDIA; Email: cst.iisc@gmail.com*

[‡]Authors have contributed equally in this work.

ABSTRACT

Conversion of carbon-di-oxide into selective hydrocarbon using stable catalyst remains a holy-grail in catalysis community. The high overpotential, stability, and selectivity in use of a single metal-based catalyst still remain a challenge. In current work, instead of using pure noble metals (Ag, Au, and Pt) as the catalyst, a novel nanocrystalline high entropy alloy (HEA: AuAgPtPdCu) has been used for conversion of CO_2 into gaseous hydrocarbons. Utilizing an approach of multi-metallic HEA, a Faradaic efficiency of about 100% towards gaseous products is obtained. The reason behind the superior catalytic activity of high entropy alloy (HEA) was established through first-principles based density functional theory (DFT) by comparing it with pristine Cu (111) surface. This is attributed to the reversal in adsorption trends for two out of the total eight intermediates - $^{*}OCH_3$ and $^{*}O$ on Cu(111) and HEA surfaces.

Proficient conversion of CO_2 into carbon fuels via electrocatalytic reduction of carbon dioxide (CO_2) can play a key role in sustaining global energy demands[1-3]. However, this practical applications of the CO_2 reduction reaction (CO_2RR) are currently challenged by the low activity and selectivity due to the high kinetic barriers and competition with the hydrogen evolution reactions in aqueous media[4-5]. There are several efforts to develop advanced catalysts with specific electronic structures, which could facilitate the CO_2 activation process with high selectivity[6-8]. Conceptually, tuning the surface area and morphology of the catalysts is extremely important[9]. The nanoparticles demonstrate improved catalytic activities with decent chemical transformation as compared to its bulk counterpart[9].

The nobel-metalcatalysts such as Au, Ag, Pt, Pd, have been demonstrated to convert CO_2 to carbon monoxide with high selectivity[10-14]. Platinum (Pt), generally considered as the active electrocatalyst for all the electrochemical reactions, generates H_2 exclusively instead of CO_2 reduction in the aqueous medium. Additionally, it is easily poisoned by CO[5]. Recently, copper (Cu) has gained more attention and focus because of its ability to convert CO_2 into higher hydrocarbon fuels[15-18]. However, copper-based materials show limited selectivity due to significant hydrogen generation. Interestingly, the bimetallic alloys of this element show an improvement in catalytic activity and selectivity however, CO and H_2 forms in most of the cases with high faradaic efficiency.[19-22]. The nanomaterials catalysts with substitution of few atoms shows selective conversion of CO_2 to carbon fuel[23]. Recently, high entropy alloys (HEAs), a simple solid solution phase, have been studied as multifunctional materials by tuning their thermal, electrical, magnetic and catalytic properties.[24-27] Their potential applications in electrocatalysis of oxygen reduction reaction[25], methanol[26], and hydrogen evolution reaction[27] have been reported. These multicomponent "cocktails" with simple crystal structure (FCC, BCC or HCP) can effectively be utilized for various functional applications, notably catalytic applications as their composition and constituents can be tuned for specific applications. This

can be done by preparing HEA containing catalytically active metals. Such kind of approach opens new area of single atom catalysts[9, 28]. These HEAs are in general highly active and used without any support but it is possible to disperse them on a support to increase the activity further utilizing the phenomenon of metal support interaction.[29-30]

Here, a unique catalyst based on combination of five active metals (Au, Ag, Pt, Pd and Cu) high entropy alloy has been developed as a 'single atom catalyst' in which the Cu atoms are stabilized by other metals in a 'FCC-facet' crystalline structures (Figure 1a). The synergistic impact on Cu with all other metals plays a key role in enhancing stability. HEA also acts as 'single atom electrocatalysis' for CO_2RR in an aqueous electrolyte. HEA is utilized as the working electrode, Pt wire as the counter electrode and CO_2 saturated K_2SO_4 as an electrolyte. Gaseous products generated during the electrochemical investigations are analyzed using gas chromatograph. To rationalize the high activity of HEAs from atomistic level, ab-initio density functional theory (DFT) calculations have been performed. It establishes the superior catalytic activity of HEAs, compared to the pristine Cu, based on the thermodynamics study.

The HEA alloy has been synthesized using an easily scalable and precise composition control route of melting and cryogrinding[31]. The XRD pattern of synthesized HEA nanoparticles reveals formation of a single-phase with face-centered cubic structure (FCC) having lattice parameter 0.3936 nm as shown in Figure 1b. Similarly, the nanocrystalline FCC structure was proven by electron diffraction ring pattern. These nanoparticles show average size of 16±10 nm as shown in Figure 1c. The HR-STEM image shown in Figure 1d reveals 001 lattice arrangements with different intensity of individual lattice, which can be assigned to different atoms. All elements (Au, Ag, Pd, Pt, and Cu) were homogeneously distributed or alloyed in single phase FCC matrix, which is proven by atom probe tomography (APT) as shown in Figure 1e, indicating homogeneous distribution of elements at atomic level. The HEA contains five elements. Therefore, interatomic effects (atoms surrounding) as well as surface oxidation

of nanoparticles were revealed using X-ray photoelectron spectroscopy. The elemental peak binding energy has been corrected with adventitious carbon C1s 284.6 eV[32]. The XPS spectra of the HEAs are shown in Figure 1f. The Pt(4f) core level shows two peaks at 71.1 ($Pt4f_{7/2}$) and 74.4 ($Pt4f_{5/2}$) eV similar to bulk Pt [33]. Au(4f) core level spectra show two peaks at 84.0 eV and 88.0 eV related to $Au(4f_{7/2})$ and $Au(4f_{5/2})$ respectively. This is again similar to bulk Au. Similarly, the binding energy (B.E.) of Pd and Cu confirms the pure metallic characteristic with binding energies similar to their bulk counterpart. Small amount of Cu^{2+} is also observed in the XPS. B.E. for $Ag3d_{5/2}$ which appears at 367.8 eV, 0.4 eV lower than metallic Ag. Clearly, there is some intrinsic charge transfer between Ag and Cu. This phenomenon is consistent with the XPS of bimetallic Au-Ag alloy as well[34]. The XPS is surface sensitive technique which gives information from few atomic layers (in depth) and Figure 1f confirmed that the AuAgPtPdCu is chemically homogeneous high entropy alloy at the surfaces of nanoparticles, which is the key for catalytic activities of NPs. Similarly, XRD and APT also proved crystal structure and overall composition respectively.

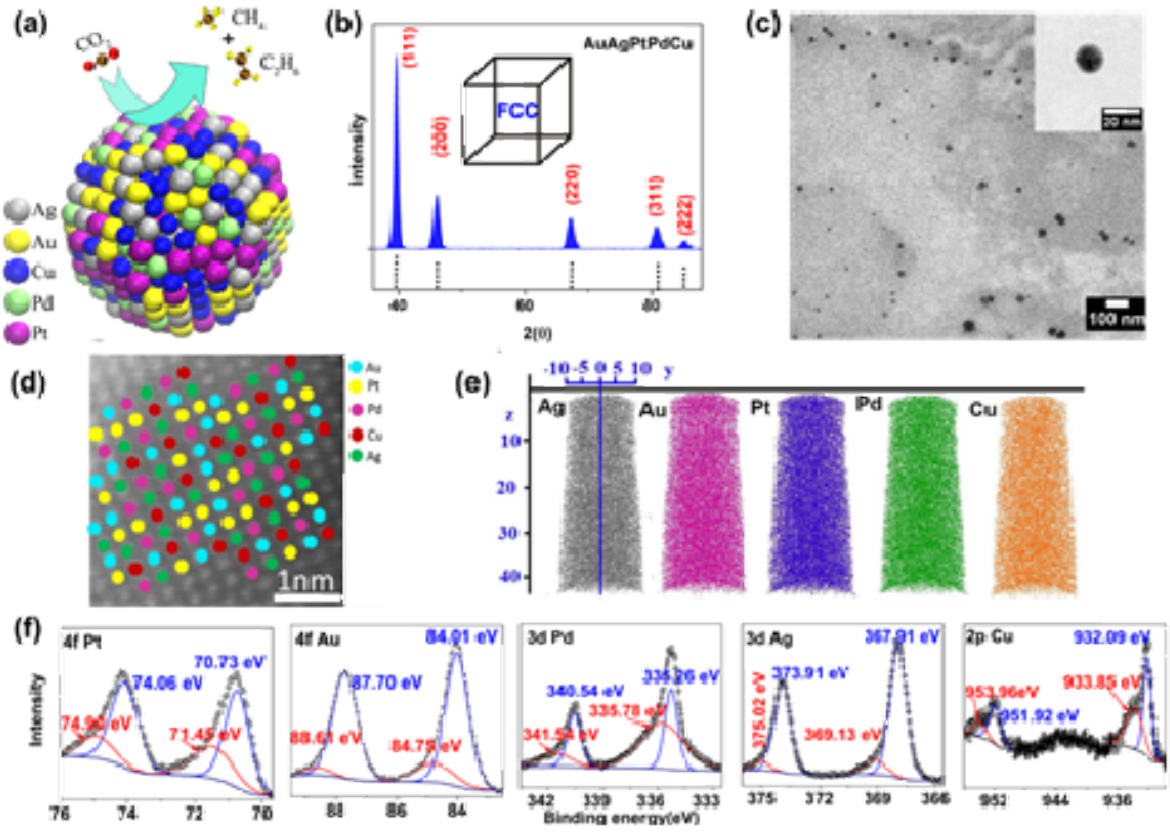

Figure 1: **(a)** Schamtic of the catalysis reaction demonstarted in current work, **(b)** X-ray diffaraction pattern of HEA alloy NPs (AuAgPtPdCu nanoparticles), **(c)** TEM bright field image of HEA nanoparticles, inset shows high magnification image of single artice. **(d)** HR-STEM image revelaing lattice with color showing different relative intensity marked with color. **(e)** chemical homogenity of Au, Ag, Pt, Pd and Cu (mapping of an atom probe microscope) **(f)** binding energy spectra of HEA nanoparticles (X-ray photoelectron spectroscopy).

Cyclic voltammetry (CV) behavior of HEA coated glassy carbon at 40 mV s^{-1} in 0.5 M K_2SO_4 is shown in Figure 2. The observed CV showed a prominent redox peak (A1/C1) at -0.13 and -0.32 V(Figure 2a) corresponding to Cu^{2+}/Cu^0redox reaction[20]. Apart from the redox peak (A1/C1), the oxidation and reduction peaks at 0.42 (A2) and 0.25V (C2) also appear, typical of Pt and Au metal behavior[35-36]. Once the potential range is restricted to the negative side (0.0 to -1.0 V), the peak A1 becomes broad and appear with a shoulder. Corresponding reduction peak (C1) does not appear in this potential range confirming the incomplete surface oxidation. Presence of the redox peak related to Cu^{2+}/Cu^0 proves that this species can play a critical role

in the catalytic activity. Therefore, the electro-reduction of CO_2 is selected as copper is the most active catalyst for this reaction[4, 15, 19-20].

Figure 2b represents linear sweep voltammetric (LSV) responses of HEA coated glassy carbon electrode containing N_2 (as blank) or CO_2 saturated (purging for 30 min) K_2SO_4 electrolyte. The considerable activity of HEA in CO_2 saturated solution is apparent. Experiments are carried out at 20 mV s^{-1} in the potential range of 0.0 to -1.0 V vs Ag/AgCl. The CO_2 reduction starts above -0.5 V, where current density rises rapidly up to -0.8 V and then decreases forming a peak at -0.8V. At -0.8V, the cathodic current density is 10.15 $mAcm^{-2}$, ~5 times higher than the N_2 saturated solution (2.2 $mAcm^{-2}$). These observations confirm the significant activity of HEA for CO_2 electroreduction. The corresponding current efficiency (CE %) for electroreduction of CO_2 at different potentials are calculated using equation S1. The highest current efficiency (81.8%) is achieved at −0.8 V (inset of Figure 2b). It is interesting to note that the electrochemical reduction CO_2 is usually carried out in a basic electrolyte such as $NaHCO_3$. However, in the case of HEA, CO_2 saturated $NaHCO_3$ (0.5 M) did not yield any activity (Supporting Figure S1(a)). Presently, the reason is unknown, but one can speculate the pH-dependent activity of HEA.

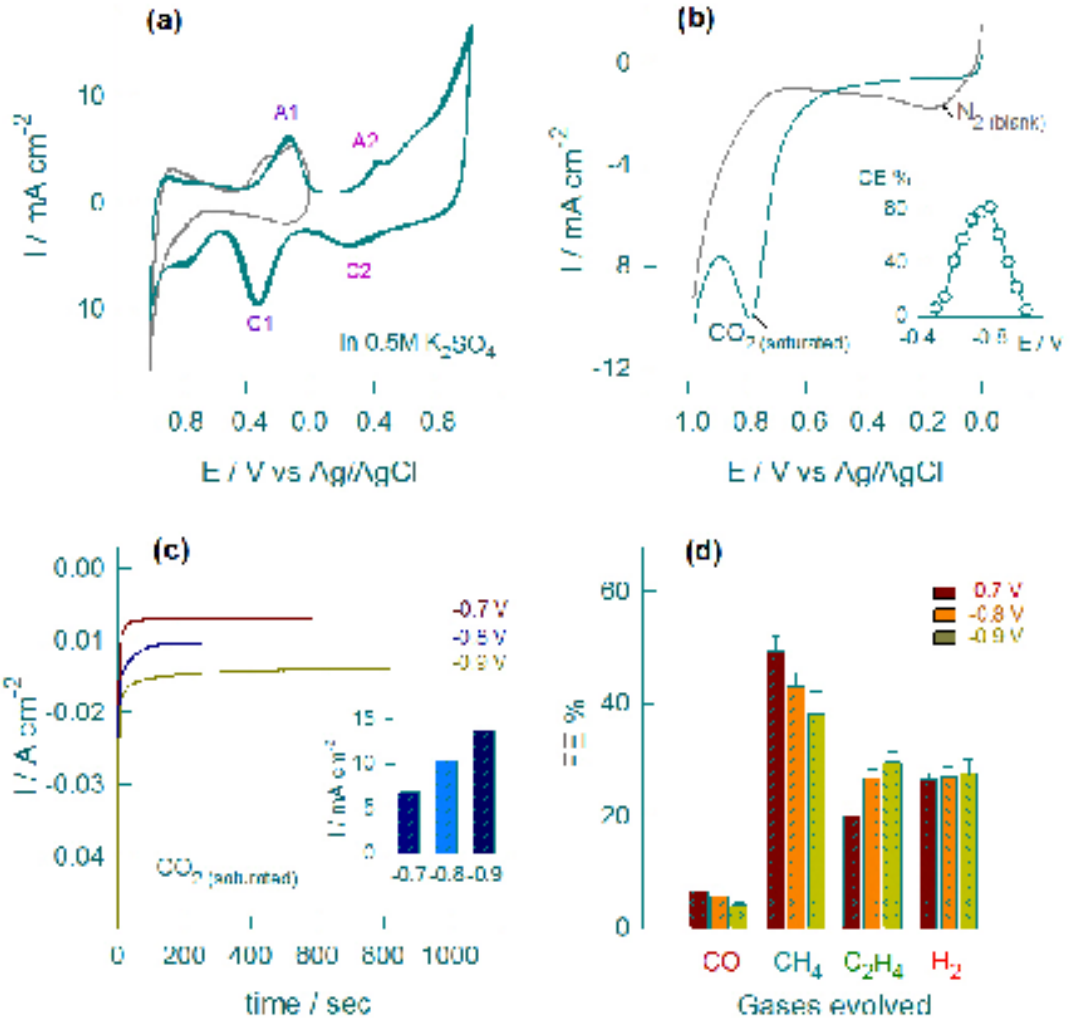

Figure 2: Cyclic voltammetric responses of high entropy alloy catalyst deposited on glassy carbon electrode in blank 0.5 M K_2SO_4 at a scan rate of 40 mV s^{-1} **(a)**, Linear sweep voltammetric response for CO_2RR (saturated for 30 mins) at a scan rate of 20 mV s^{-1} with N_2 purged electrolyte and inset is the plot of current efficiency (CE%) vs. potential **(b)**, Comparative chronoamperometric responses in CO_2 saturated electrolyte at different potentials (-0.7, -0.8 and -0.9 V) for 1000 seconds with respective current density as inset **(c)**. Bar diagram (with errors) for the faradaic efficiencies of their respective carbonaceous species and hydrogen gaseous products **(d)**.

Steady-state current responses of HEA in CO_2 saturated electrolyte at a various potential (-0.7, -0.8 and -0.9V) is also shown in Figure 2c. Obtained steady state current densities are -6.83 $mAcm^{-2}$ (at -0.7V), -10.31 $mAcm^{-2}$ (at -0.8V) and -13.81 $mAcm^{-2}$ (at -0.9 V), respectively. A bar diagram indicating the impressive CO_2 electroreduction activity of HEA at -0.9 V, is shown in the inset of Figure 2c. The major gaseous products on HEA are CO, CH_4, C_2H_4 and H_2,

similar to the copper-based electrocatalysts[37]. It is worth noticing that in spite of many elements present in the catalyst, the catalytic effect is depicted only by the copper confirming that other elements are only providing the synergistic effect. Faradaic efficiencies (FE %), calculated as per the equation (S2), are shown in Figure 2d. FE % of CO was ~7 %, at-0.7 V which deceased to 4.0% at -0.9 V. Comparatively, the formation of CH_4 and C_2H_4 was predominantly occurred with FE % up to 49.4% and 19.9 % (at -0.7V), 42.9 % and 26.6 % (at -0.8 V) and 38.0% and 29.5% (at -0.9 V), respectively. The FE % for hydrogen on HEA catalyst is about 26.4% which does not change significantly at other potentials. Importantly, the total faradaic efficiency is 100 % for the gaseous products combined. This confirms that there is zero or negligible liquid product formation highlighting the unique capability of HEA catalyst. A detailed catalytic activity comparison of HEA with other reported catalysts is given in Table T1 (in supporting information). One can notice that HEA performs the best in terms of low applied voltage and striking hydrocarbon efficiency. Long term stability of HEA is studied using chronoamperometry for 5 hours in K_2SO_4 solution (Figure S1(b)). Electrolyte is continuously bubbled with CO_2 during the experiment. Initially, current decreases reaching a steady state, which remains constant for 5 hours. This highlights the stability of HEA.

To gain an insight into the reaction, we have performed DFT calculations. We compared the catalytic activity of the multicomponent HEA with Cu to bring about the salient features of the HEA as catalysts for CO_2RR. The aim is to provide the mechanisms for excellent catalytic activity of HEA. The optimized lattice parameters of Cu are found to be, a = b = c = 3.63 Å (Figure S2a), which is in excellent agreement with the previous reports[38]. The (111) facet was chosen for calculations, as it is the most stable facet of the FCC metals. The supercell size of the Cu (111) surface was selected as 5x3x1 to get all the possible adsorbing sites, which are also present in the HEAs (Figure S2 and S3(a)). The unit cell of HEAs contained 120 atoms, with the constituent elements - Pt, Pd, Ag, Au and Cu, being equal in proportion (20 % each).

The method for generation of the structure of HEA utilized in the present study is described in detail in the supporting information file. Based on experimental composition, the Au:Ag:Pt:Pd:Cu=1:1:1:1:1composition was chosen for simulation Then quantification of the catalytic activity of pristine Cu was performed using the scheme provided by Norskov *et al.*[39-40] For this purpose, the adsorption energies of all the intermediates involved in the eight-step CO_2RR (equations S1-S8) was calculated from DFT using the expressions given in supplementary information (equations S9-S15). Subsequently, these intermediate adsorption energies were converted into Gibb's free energies of adsorption[39, 41] using:

$$\Delta G_{inter}^{ads} = \Delta E_{inter}^{ads} + \Delta ZPE - T\Delta S - \Delta G_U \qquad (1)$$

where ΔZPE is the difference in zero-point energies, ΔS is the change in entropy due to vibrational contributions, and $\Delta G_U = -eU$, where U is the applied electrode potential. The values of zero-point energies and entropies for the intermediates and reference molecules have been taken from the reported literature[39]. The complete free-energy reaction profile for CO_2RR is given in Figure S5. The reaction profile at 0 V is shown by black curves, where three elementary steps are endoergic, i.e., $^*CO$ to $^*CHO$, $^*OCH_3$ to $^*O$, and the final step involves the release of a water molecule from $^*OH$ intermediate. Out of these three, the elementary step for the conversion of OCH_3 into O intermediate has the highest barrier of 1.91 eV and is, therefore, the rate-determining step (RDS) for CO_2RR on Cu (111) surface. This barrier is also the theoretical limiting potential for the reduction reaction on pristine Cu surface, as at U = -1.91 V, all the elementary steps become exoergic. We then extended this thermodynamic study to the HEA system. In this case, there is a possibility of a large number of catalytic centers due to the five elements being present randomly on the surface. In order to mitigate this problem, we chose only one catalytic center from electronic principles of designing catalyst, i.e., based on position of d-band center (E_{dBC}). In general, the activity of any catalytic reaction is related to the d-band center of the metal under consideration[42]. Therefore, d-band centers of all the atoms

present on the topmost layer of the HEA slab (Figure S3(a)) have been plotted in both the up and down spin configurations in Figure S6. From this plot, we notice that Pd^{11} atom has the value of E_{dBC} closest to the Fermi level (E_F) in both spin configurations. Hence it was chosen as the catalytic center for CO_2RR study. Pd^{11} is also adjacent to a Cu atom on the surface (Cu^7; Figure S3(a)), which would enhance the catalytic activity of Pd^{11} center. The free-energy profile for the HEA system is shown in Figure 3. The two endoergic reactions, which are same as in the case of pristine Cu (111) surface are $^*CO$ to $^*CHO$, and $^*OCH_3$ to $^*O$ conversions.

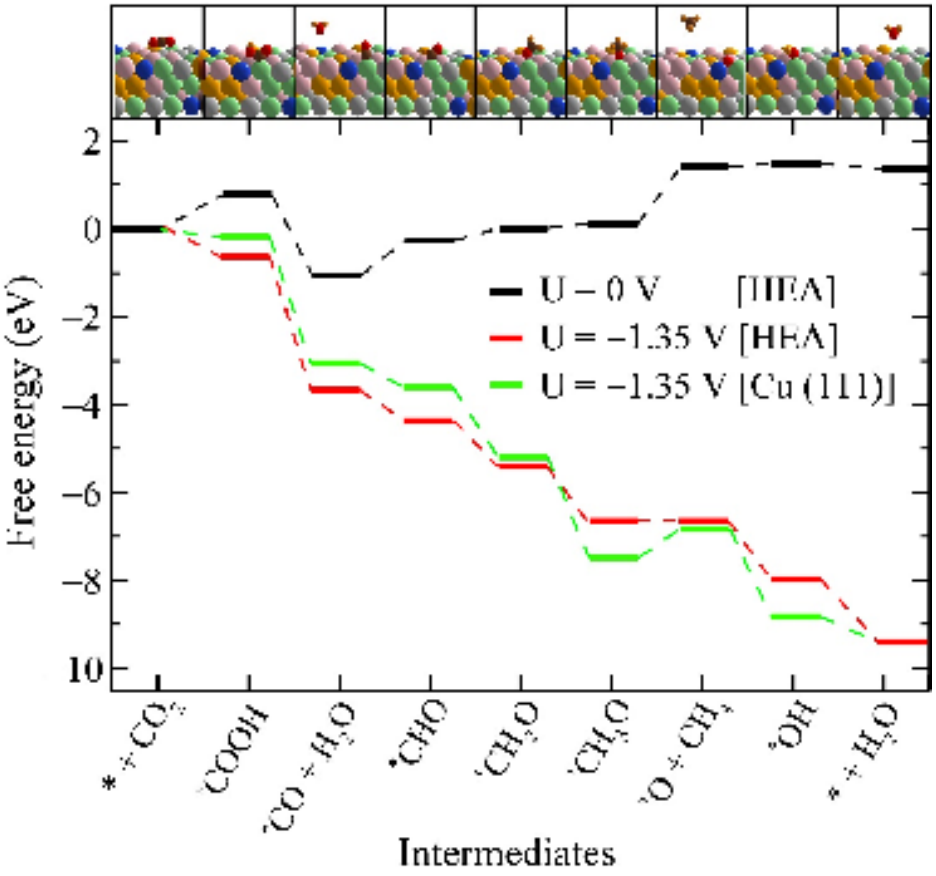

Figure 3: Free energy diagram of CO_2RR on AuAgPtPdCu HEA surface. Optimized structures of all the intermediates on HEA surface are shown in the inset. Grey, green, pink, yellow, blue, brown, red and orange spheres represent Pt, Pd, Ag, Au, Cu, C, O, and H atoms, respectively.

However, the barriers in this system are reduced significantly, e.g., 0.73 eV for the 3rd elementary step and 1.35 eV for the 6th elementary step. Hence, at a potential of -1.35 V, the

reaction profile becomes downhill in energy. The free energy profile of Cu (111) surface is also plotted at the same potential in Figure 3, which is depicted by green lines. It is clear that at this potential, the step of $^{*}OCH_3$ to $^{*}O$ conversion is still uphill, requiring more external potential to overcome this barrier. Therefore, the theoretical limiting potential for HEA system is lower than that of pristine Cu metal, implying the thermodynamic favoring of CO_2RR on the HEA surface over the Cu (111) surface. This is in agreement with the experimental observations. The reduced theoretical limiting potential for HEA system can be attributed to the destabilization of $^{*}OCH_3$ intermediate and stabilization of the $^{*}O$ intermediate on the HEA surface, compared to the Cu (111) surface. The extra stabilization of $^{*}O$ intermediate on the HEA surface may be because both Pd^{11} and Cu^{7} atoms are bonded to the O atom. This behavior can be explained from the partial density of states (PDOS) plotted in Figures S7 and S8 for $^{*}OCH_3$ and $^{*}O$ intermediates, respectively. While in the case of $^{*}OCH_3$ intermediate on Cu (111) surface, the hybridized states of O and Cu^{96} atom are filled and more broadened while all hybridized states of O and Pd^{11} are sharply peaked. Moreover, one state in down spin configuration is unfilled on HEA surface. This would lead to stronger binding of OCH_3 on the Cu (111) surface. Cu^{96} and Pd^{11} are the sites through which OCH_3 intermediate gets adsorbed on the two surfaces under consideration. Similarly, the states of O intermediate on Cu (111) are sharply peaked, while those on the HEA surface are broader, resulting in better adsorption of O intermediate on HEA than on the Cu (111) surface. In this case, O adsorbs through 3 atoms (hcp type of adsorption site) – Cu^{88}, Cu^{96}, and Cu^{108} atoms on pristine Cu slab, and Cu^{7}, Cu^{12}, and Pd^{11} atoms on the HEA slab.

In conclusion, we demonstrated that the unprecedented catalytic activity of cryomilled prepared nanocrystalline equiatomic Au-Ag-Pt-Pd-Cu high entropy alloy for efficient electrochemical reduction of CO_2RR. Collective characterizations such as XRD, HRTEM, and XPS reveal the atomic distribution in the HEA. In spite of many elements present in the

catalyst, the electrocatalytic activity is predominantly described by the presence of redox active Cu metal (Cu^{2+}/Cu^{0}), and other metals only provide a synergistic effect. Complete 100% conversion of CO_2 to gaseous products highlights the uniqueness HEA and making it different from Cu metal alone. The density functional theory (DFT) studies establish the HEAs as a superior catalyst, compared to the pristine Cu metal, based on the free energy calculations of intermediates.

ASSOCIATED CONTENT

The Supporting Information is available free of charge on the ACS Publications websites. Detailed synthesis procedure, experimental and instrumentation details, computational DFT studies and calculations (PDF).

AUTHOR INFORMATION

**Corresponding Authors*

E-mail: ssharma@iitgn.ac.in (S.S*), abhishek@iisc.ac.in (A.K.S*), cst.iisc@gmail.com (C.S.T*), kbiswas@iitk.ac.in (K.B*)

Notes

The authors declare no competing financial interest.

ACKNOWLEDGMENTS

S.S. and S.N. acknowledges DST-SERB (EMR/2016/000806) project for the funding and fellowship. A.P, R.K. and A.K.S. acknowledge Materials Research Centre, Solid State and Structural Chemistry Unit, and Supercomputer Education and Research Centre for providing the computational facilities.

REFERENCES

(1) Costentin, C.; Roberta, M.; Saveant, J.-M. Catalysis of the Electrochemical Reduction of Carbon dioxide. *Chem. Soc. Rev.,* **2013,** *42*, 2423-2436.

(2) Qiao, J.; Liu, Y.; Hong, F.; Zhang, J. A Review of Catalysts for the Electroreduction of Carbon Dioxide to Produce Low-Carbon Fuels. *Chem. Soc. Rev.,* **2014,** *43*, 631-675.

(3) Liu, C.; Colon, B. C.; Ziesack, M.; Silver, P. A.; Nocera, D. G. Water Splitting–Biosynthetic System with CO_2 Reduction Efficiencies Exceeding Photosynthesis. *Science* **2016,** *352*, 1210–1213.

(4) Li, C. W.; Ciston, J.; Kanan, M. W. Electroreduction of Carbon Monoxide to Liquid Fuel on Oxide-Derived Nanocrystalline Copper. *Nature* **2014,** *508*, 504-507.

(5) Kuhl, K. P.; Hatsukade, T.; Cave, E. R.; Abram, D. N.; Kibsgaard, J.; Jaramillo, T. F. Electrocatalytic Conversion of Carbon Dioxide to Methane and Methanol on Transition Metal Surfaces. *J. Am. Chem. Soc.,* **2014,** *136*, 14107–14113.

(6) Cheng, Y.; Zhao, S.; Johannessen, B.; Veder, J.-P.; Saunders, M.; Rowles, M. R.; Cheng, M.; Liu, C.; Chisholm, M. F.; Marco, R. D.; Cheng, H.-M.; Yang, S.-Z.; Jiang, S. P. Atomically Dispersed Transition Metals on Carbon Nanotubes with UltraHigh Loading for Selective Electrochemical Carbon Dioxide Reduction. *Adv. Mater., 2018,* **2018,** *30*, 1706287-1706293.

(7) Mori, K.; Taga, T.; Yamashita, H. Isolated Single-Atomic Ru Catalyst Bound on a Layered Double Hydroxide for Hydrogenation of CO_2 to Formic Acid. *ACS Catal.,* **2017,** *7*, 3147−3151.

(8) Back, S.; Lim, J.; Kim, N.-Y.; Kim, Y.-H.; Jung, Y. Single-Atom Catalysts for CO_2 Electroreduction with Significant Activity and Selectivity Improvements. *Chem. Sci.,* **2017,** *8*, 1090-1096.

(9) Wang, A.; Li, J.; Zhang, T. Heterogeneous Single-Atom Catalysis. *Nat. Rev. Chem* **2018,** *2* (6), 65-81.

(10) Zhu, W.; Michalsky, R.; Metin, O.; Lv, H.; Guo, S.; Wright, C. J.; Sun, X.; Peterson, A. A.; Sun, S. Monodisperse Au nanoparticles for selective electrocatalytic reduction of CO_2 to CO. *J. Am. Chem. Soc.,* **2013,** *135*, 16833- 16836.

(11) Ma, M.; Trześniewski, B. J.; Xie, J.; Smith, W. A. Selective and Efficient Reduction of Carbon Dioxide to Carbon Monoxide on Oxide-Derived Nanostructured Silver Electrocatalysts. *Angew. Chem. Int. Ed.,* **2016,** *55* (33), 9748-9752.

(12) Mistry, H.; Reske, R.; Zeng, Z.; Zhao, Z. J.; Greeley, J.; Strasser, P.; Cuenya, B. R. Exceptional Size-Dependent Activity Enhancement in the Electroreduction of CO_2 over Au Nanoparticles. *J. Am. Chem. Soc.,* **2014,** *136*, 16473-16476.

(13) Gao, D.; Zhou, H.; Wang, J.; Miao, S.; Yang, F.; Wang, G.; Wang, J.; Bao, X. Size-Dependent Electrocatalytic Reduction of CO_2 over Pd Nanoparticles. *J. Am. Chem. Soc.,* **2015,** *137*, 4288-4291.

(14) Kim, C.; Jeon, H. S.; Eom, T.; Jee, M. S.; Kim, H.; Friend, C. M.; Min, B. K.; Hwang, Y. J. Achieving Selective and Efficient Electrocatalytic Activity for CO_2 Reduction Using Immobilized Silver Nanoparticles. *J. Am. Chem. Soc.,* **2015,** *137*, 13844−13850.

(15) Manthiram, K.; Beberwyck, B. J.; Alivisatos, A. P. Enhanced Electrochemical Methanation of Carbon Dioxide with a Dispersible Nanoscale Copper Catalyst. *J. Am. Chem. Soc.,* **2014,** *136*, 13319–13325.

(16) Reske, R.; Mistry, H.; Behafarid, F.; Cuenya, B. R.; Strasser, P. Particle Size Effects in the Catalytic Electroreduction of CO_2 on Cu Nanoparticles. *J. Am. Chem. Soc.,* **2014,** *136*, 6978-6989.

(17) Xie, J.-F.; Huang, Y.-X.; Li, W.-W.; Song, X.-N.; Xiong, L.; Y, H.-Q. Efficient Electrochemical CO_2 Reduction on a Unique Chrysanthemum-Like Cu Nanoflower Electrode and Direct Observation of Carbon Deposite. *Electrochim. Acta* **2014,** *139*, 137-144.

(18) Raciti, D.; Livi, K. J.; Wang, C. Highly Dense Cu Nanowires for Low-Overpotential CO_2 Reduction. *Nano Lett.,* **2015,** *15*, 6829–6835.

(19) Kim, D.; Resasco, J.; Yu, Y.; Asiri, A. M.; Yang, P. Synergistic Geometric and Electronic Effects for Electrochemical Reduction of Carbon Dioxide Using Gold–Copper Bimetallic Nanoparticles. *Nat. Commun.,* **2014,** *5*, 4948.

(20) Li, Q.; Fu, J.; Zhu, W.; Chen, Z.; Shen, B.; Wu, L.; Xi, Z.; Wang, T.; Lu, G.; Zhu, J.-j.; Sun, S. Tuning Sn-Catalysis for Electrochemical Reduction of CO_2 to CO via the Core/Shell Cu/SnO_2 Structure. *J. Am. Chem. Soc.,* **2017,** *139*, 4290-4293.

(21) Ma, S.; Sadakiyo, M.; Heima, M.; Luo, R.; Haasch, R. T.; Gold, J. I.; Yamauchi, M.; Kenis, P. J. A. Electroreduction of Carbon Dioxide to Hydrocarbons Using Bimetallic Cu−Pd Catalysts with Different Mixing Patterns. *J. Am. Chem. Soc.* **2017,** *139*, 47-50.

(22) Liu, K.; Ma, M.; Wu, L.; Valenti, M.; Cardenas-Morcoso, D.; Hofmann, J. P.; Bisquert, J.; Gimenez, S.; Smith, W. A. Electronic Effects Determine the Selectivity of Planar Au−Cu Bimetallic Thin Films for Electrochemical CO_2 Reduction. *ACS Appl. Mater. Interfaces* **2019,** *11*, 16546−16555.

(23) Zhou, S.; Varughese, B.; Eichhorn, B.; Jackson, G.; McIlwrath, K. Pt–Cu Core–Shell and Alloy Nanoparticles for Heterogeneous NOx Reduction: Anomalous Stability and Reactivity of a Core–Shell Nanostructure. *Angew. Chem. Int. Ed.* **2005,** *44* (29), 4539-4543.

(24) Ye.Y.F; Wang.Q; Lu.J; Liu.C.T; Yang.Y. High-Entropy Alloy: Challenges And Prospects. *Materials Today* **2016,** *19* (6), 349-362.

(25) Löffler, T.; Meyer, H.; Savan, A.; Wilde, P.; Manjón, A. G.; Chen, Y.-T.; Ventosa, E.; Scheu, C.; Ludwig, A.; Schuhmann, W. Discovery of a Multinary Noble Metal–Free Oxygen Reduction Catalyst. *Adv. Energy Mater.* **2018,** *8* (34), 1802269-1802276.

(26) Wang, A.-L.; Wan, H.-C.; Xu, H.; Ye-Xiang; Li, T. G.-R. Quinary PdNiCoCuFe Alloy Nanotube Arrays as Efficient Electrocatalysts for Methanol Oxidation. *Electrochim. Acta* **2014,** *127*, 448-453.

(27) Zhang, G.; Ming, K.; Kang, J.; Huang, Q.; Zhang, Z.; Zheng, X.; Bi, X. High Entropy Alloy as a Highly Active and Stable Electrocatalyst for Hydrogen Evolution Reaction. *Electrochim. Acta* **2018,** *279*, 19-23.

(28) Qiao, B.; Wang, A.; Yang, X.; Allard, L. F.; Jiang, Z.; Cui, Y.; Liu, J.; Li, J.; Zhang, T. Single-atom Catalysis of CO Oxidation Using Pt1/FeO_x. *Nature Chem.* **2011,** *3*, 634.

(29) Kumari, N.; Sinha, N.; Haider, M. A.; Basu, S. CO_2 Reduction to Methanol on CeO_2 (110) Surface: A Density Functional Theory Study. *Electrochim. Acta* **2015,** *177*, 21-29.

(30) Kumari, N.; Haider, M. A.; Agarwal, M.; Sinha, N.; Basu, S. Role of Reduced CeO_2 (110) Surface for CO_2 Reduction to CO and Methanol. *J. Phys. Chem. C* **2016,** *120*, 16626−16635.

(31) Kumar, N.; Tiwary, C. S.; Biswas, K. Preparation of Nanocrystalline High-Entropy Alloys via Cryomilling of Cast Ingots. *J. mater. Sci.* **2018,** (19), 12.

(32) Yu, X.; Hantsche, H. Some Aspects of the Charging Effect in Monochromatized Focused XPS. *Fresenius J. Anal. Chem.* **1993,** *346* (1), 233-236.

(33) Shyu, J. Z.; Otto, K. Identification of Platinum Phases on γ-alumina by XPS. *Appl. Surf. Sci.* **1988,** *32* (1), 246-252.

(34) Wang, A.-Q.; Liu, J.-H.; Lin, S. D.; Lin, T.-S.; Mou, C.-Y. A Novel Efficient Au–Ag Alloy Catalyst System: Preparation, Activity, and Characterization. *J. Catal.* **2005,** *233* (1), 186-197.

(35) Ge, X.; Wang, R.; Liu, P.; Ding, Y. Platinum-Decorated Nanoporous Gold Leaf for Methanol Electrooxidation. *Chem. Mater.,* **2007,** *19*, 5927-5829.

(36) Ballarin, B.; Gazzano, M.; Scavetta, E.; Tonell, D. One-Step Electrosynthesis of Bimetallic Au-Pt Nanoparticles on Indium Tin Oxide Electrodes: Effect of the Deposition Parameters. *J. Phys. Chem. C* **2009,** *113*, 15148-15154.

(37) Hori, Y.; Murata, A.; Takahashi, R. Formation of Hydrocarbons in the Electrochemical Reduction of Carbon Dioxide at a Copper Electrode in Aqueous Solution. *J. Chem. Soc., Faraday Trans. 1,* **1989,** *85* (8), 2309-2326.

(38) Straumanis, M. E.; Yu, L. S. Lattice Parameters, Densities, Expansion Coefficients and Perfection of Structure of Cu and of Cu-In α Phase. *Acta Cryst.,* **1969,** *A25*, 676-682.

(39) Peterson, A. A.; Abild-Pedersen, F.; Studt, F.; Rossmeisla, J.; Nørskov, J. K. How Copper Catalyzes the Eletroreduction of Carbon Dioxide into Hydrocarbon Fuels. *Energy Environ. Sci.,* **2010,** *3*, 1311-1315.

(40) Peterson, A. A.; Norskov, J. K. Activity Descriptors for CO_2 Electroreduction to Methane on Transition-Metal Catalysts. *J. Phys. Chem. Lett.,* **2012,** *3*, 251–258.

(41) Kumar, R.; Das, D.; Singh, A. K. C_2N/WS_2 Van der Waals type-II Heterostructure as a Promising Water Splitting Photocatalyst. *J. Catal.* **2018,** *359*, 143-150.

(42) Norskov, J. K.; Abild-Pedersen, F.; Studt, F.; Bligaard, T. Density Functional Theory in Surface Chemistry and Catalysis. *Proc. Natl. Acad. Sci.,* **2011,** *108*, 937-943.

TOC